



Global tree intrinsic water use efficiency is enhanced by increased atmospheric CO₂ and modulated by climate and plant functional types

Justin M. Mathias^{a,1}  and Richard B. Thomas^a 

^aDepartment of Biology, West Virginia University, Morgantown, WV 26506

Edited by Elizabeth Ainsworth, Agricultural Research Service, Urbana, IL, and approved January 4, 2021 (received for review July 7, 2020)

We conducted a meta-analysis of carbon and oxygen isotopes from tree ring chronologies representing 34 species across 10 biomes to better understand the environmental drivers and physiological mechanisms leading to historical changes in tree intrinsic water use efficiency (iWUE), or the ratio of net photosynthesis (A_{net}) to stomatal conductance (g_s), over the last century. We show a ~40% increase in tree iWUE globally since 1901, coinciding with a ~34% increase in atmospheric CO₂ (C_a), although mean iWUE, and the rates of increase, varied across biomes and leaf and wood functional types. While C_a was a dominant environmental driver of iWUE, the effects of increasing C_a were modulated either positively or negatively by climate, including vapor pressure deficit (VPD), temperature, and precipitation, and by leaf and wood functional types. A dual carbon–oxygen isotope approach revealed that increases in A_{net} dominated the observed increased iWUE in ~83% of examined cases, supporting recent reports of global increases in A_{net} , whereas reductions in g_s occurred in the remaining ~17%. This meta-analysis provides a strong process-based framework for predicting changes in tree carbon gain and water loss across biomes and across wood and leaf functional types, and the interactions between C_a and other environmental factors have important implications for the coupled carbon–hydrologic cycles under future climate. Our results furthermore challenge the idea of widespread reductions in g_s as the major driver of increasing tree iWUE and will better inform Earth system models regarding the role of trees in the global carbon and water cycles.

tree rings | stable isotopes | carbon | oxygen | intrinsic water use efficiency

How terrestrial plants respond to more frequent, and often prolonged, environmental stressors will have profound impacts on, and feedbacks to, the Earth–climate system at regional to continental scales (1, 2). Central to these feedbacks are plant stomata, microscopic pores on the leaves of plants that act as a control valve over the fluxes of carbon dioxide (C_a) into the leaf during photosynthesis and water vapor (H_2O) out of the leaf during transpiration. Importantly, changes in stomatal aperture do not affect the fluxes of C_a and H_2O equally, as the sum of resistances for the diffusion of C_a from the atmosphere to mesophyll cells where Rubisco is located are much greater than those for H_2O from the surface of leaf mesophyll cells to the atmosphere (3). Indeed, as stomatal aperture changes, so does water use efficiency (WUE), or the ratio of C_a uptake to H_2O released from the leaf to canopy scale (4). Consequently, understanding the environmental factors driving changes in leaf physiology is of paramount concern in the context of climate change as small changes in tree WUE can have major effects on the carbon and hydrologic cycles over large geographical areas (1, 5).

Approaches using tree ring carbon isotopes (6–9), eddy-flux measurements (4, 9, 10), atmospheric carbon isotope composition analysis (11), and Earth system modeling techniques (9–13) have shown trends of recently increasing WUE. These increases can occur by stimulation of leaf photosynthetic rates (A_{net}) (14, 15), reduced stomatal conductance to water (g_s) (14, 15), or some combination of the two. A fundamental physiological response

found in numerous C_a enrichment experiments is that WUE of many plants is improved as a result of increasing C_a stimulating photosynthesis and causing partial stomatal closure (14, 16). However, environmental factors distinct from C_a , such as vapor pressure deficit (VPD), precipitation, and temperature, have independent effects on A_{net} and g_s and, therefore, may modulate the response of WUE to rising C_a , especially across functionally distinct plant groups with differences in wood anatomy (9) and leaf morphology (17). Despite this, few studies have thoroughly examined the effects of multiple environmental factors over controls of WUE, and even fewer have considered the underlying component parts, A_{net} and g_s (9, 13, 17–20). This has, in part, been due to the complexity of partitioning H_2O gas fluxes at ecosystem scales (21), in addition to the difficulty in attributing changes in isotopically derived intrinsic water use efficiency (iWUE) (the ratio of A_{net} to stomatal conductance to water, g_s) to A_{net} or g_s without the accompaniment of physiological measurements (18, 19).

A promising technique couples carbon isotopically derived estimates of iWUE with oxygen isotope leaf water enrichment above source water ($\Delta^{18}O_{\text{lw}}$; derived from tree ring $\delta^{18}O$ and source water $\delta^{18}O$ assumed to be $\sim\delta^{18}O_{\text{precipitation}}$) to provide a qualitative attribution of changes in iWUE to underlying A_{net} and g_s (9, 20, 22–29). As $\Delta^{18}O_{\text{lw}}$ is inversely related to g_s (26–30), if increases in iWUE were due to increases in A_{net} , then $\Delta^{18}O_{\text{lw}}$ should be constant or decrease with iWUE. However, if increases in iWUE were due to decreases in g_s , or a combination of a decrease in g_s and an increase in A_{net} , $\Delta^{18}O_{\text{lw}}$ would increase

Significance

Changes in tree physiology driven by environmental change can alter the balance of forest ecosystem carbon and water fluxes. We performed a meta-analysis of published tree ring literature, comprising 36 different species across 84 sites globally, to show stimulated leaf photosynthesis, not reduced stomatal conductance, is primarily responsible for recently increasing tree intrinsic water use efficiency (iWUE), which integrates the balance between carbon and water fluxes. Furthermore, we show trends in tree iWUE are similar in magnitude to the increase in atmospheric CO₂ over the 20th century and that climate interacts with CO₂ to modulate tree iWUE. These findings will help to guide efforts of refining the role of forests in process-based models under future environmental change.

Author contributions: J.M.M. and R.B.T. designed research, performed research, analyzed data, and wrote the paper.

The authors declare no competing interest.

This article is a PNAS Direct Submission.

Published under the PNAS license.

¹To whom correspondence may be addressed. Email: justinmathias@ucsb.edu.

This article contains supporting information online at <https://www.pnas.org/lookup/suppl/doi:10.1073/pnas.2014286118/-DCSupplemental>.

Published February 8, 2021.

with iWUE (9, 25, 30). As such, there currently exists a wealth of previously untapped long-term records of tree physiological responses to environmental change within numerous dendrochronological studies from around the world, providing a historical view of how iWUE has changed globally over the last century. In this analysis, we 1) synthesize published data from tree ring carbon and oxygen isotope chronologies to examine global trends in tree ring-derived iWUE, 2) identify those environmental factors, and their interactions, that best explain multidecadal to centurial trends in iWUE, and 3) investigate the potential underlying changes in A_{net} and g_s through an analysis of coupled tree ring-derived iWUE and $\Delta^{18}\text{O}_{\text{lw}}$ over time (9, 20, 22, 23, 25).

Using 113 unique tree ring carbon and oxygen isotope chronologies comprising 36 different species across 84 sites globally (Fig. 1A and SI Appendix, Table S1), we show tree-level iWUE increased, on average, by $\sim 40\%$ ($0.35\% \text{ y}^{-1}$, $\text{iWUE} = 0.23 \cdot \text{y} - 369.16$) over the last century (1901–2015) (Fig. 1B). We statistically identified a breakpoint in the combined iWUE chronology at 1963, after which iWUE increased linearly at a rate of $0.39 \pm 0.01 \mu\text{mol CO}_2\text{-mol}^{-1} \text{ H}_2\text{O}\cdot\text{y}^{-1}$ ($1.67\% \text{ y}^{-1}$), or ~ 3.9 times faster than the previous 63 y ($F = 207.14$, $P < 0.0001$) (Fig. 1B and SI Appendix, Fig. S1). This change in the rate at which tree iWUE increased after 1963 coincided with a statistical breakpoint in C_a at 1969 where CO_2 began increasing 4.1 times faster than between 1901 and 1969 (SI Appendix, Fig. S2) (31), and is similar to the trend in iWUE from a recent global synthesis by Adams et al. (32) who also showed a similar breakpoint in the 1960s. When considering individual chronologies, the increases in iWUE were widespread, with 93% (105 of 113 chronologies) of those examined having positive trends over 1901–2015 and 84% (95 of 113) of those examined having positive trends over 1963–2015 (SI Appendix, Table S1). These data for trees during the Anthropocene spanning 10 biomes in six continents that represent a spectrum of leaf and wood types reinforce reports of increasing iWUE in the United States (9), Europe (6, 8), and tropical forests (7), in addition to a recent compilation of global iWUE trends (32).

Globally, differences in vegetation physiognomy may have large impacts on iWUE, and despite much work examining plant physiological processes within biomes, there have been few large-scale comparisons of historical tree iWUE across biomes at a global scale (6, 8, 9, 12, 32). In this study, we found the rate of increase of iWUE from 1963 to 2015 differed among the 10 biomes represented ($F = 7.21$, $P < 0.001$) and ranged between $0.101 \pm 0.07 \mu\text{mol CO}_2\text{-mol}^{-1} \text{ H}_2\text{O}\cdot\text{y}^{-1}$ for trees growing in deserts and xeric shrublands to $0.611 \pm 0.07 \mu\text{mol CO}_2\text{-mol}^{-1} \text{ H}_2\text{O}\cdot\text{y}^{-1}$ for Mediterranean forests, woodlands, and scrub (SI Appendix, Fig. S3A and Table S2). Like deserts and xeric shrublands, the rate of

iWUE increase since 1963 for trees growing in the tundra and temperate grasslands, savannas, and shrublands was low, with a mean across the three biomes of $0.131 \mu\text{mol CO}_2\text{-mol}^{-1} \text{ H}_2\text{O}\cdot\text{y}^{-1}$. All other biomes exhibit mean rates of iWUE increase after 1963 greater than $0.409 \mu\text{mol CO}_2\text{-mol}^{-1} \text{ H}_2\text{O}\cdot\text{y}^{-1}$ (SI Appendix, Table S2). Furthermore, mean iWUE over 1963–2015 ranged from a low of $59.9 \mu\text{mol CO}_2\text{-mol}^{-1} \text{ H}_2\text{O}$ in tropical and subtropical moist broadleaf forests to a high of $91.5 \mu\text{mol CO}_2\text{-mol}^{-1} \text{ H}_2\text{O}$ in temperate conifer forests (SI Appendix, Fig. S3A).

When considering changes in iWUE since 1963 with respect to wood anatomy, the rate of iWUE increase was $\sim 21\%$ higher for conifers relative to diffuse porous trees ($P = 0.022$), but we found no difference in the rate of iWUE increase between conifer trees and ring porous trees ($P = 0.61$) or between diffuse porous trees and ring porous trees ($P = 0.27$) (SI Appendix, Fig. S4A). Our results are similar to climate-corrected iWUE trends from tree rings presented by Frank et al. (6) in European forests, but are in contrast to work by Saurer et al. (33) and Wang et al. (34) using tree rings and flux tower measurements, respectively, who showed broadleaf deciduous trees (i.e., ring porous and diffuse porous) in the Northern hemisphere having greater rates of increase in iWUE than conifer trees over the last century. It is important to note, however, that minor discrepancies among absolute iWUE values and their trends over time in these studies when compared to ours may have resulted from the formulation (i.e., our inclusion of a photorespiratory term) (35) and methodology differences (i.e., tree ring, flux tower) (36). We found no differences in the rate of iWUE increase since 1963 among trees with different leaf functional types ($F = 1.05$, $P = 0.37$) (SI Appendix, Fig. S4C). Additionally, we found mean iWUE during 1963–2015 was different among all wood types ($F = 782.96$, $P < 0.001$), being the highest in conifer species and lowest in ring porous species (SI Appendix, Fig. S4B), consistent with recent findings from 12 tree species at eight forested sites in the United States (9). Of important note, the patterns in mean iWUE for each wood type fall along a gradient of hydraulic conductivity and safety trade-offs (37). Conifer trees, which have relatively low hydraulic conductivity, but are more resistant to drought induced cavitation and embolism, had the highest mean iWUE, in contrast to ring porous trees, which have higher hydraulic conductivity, but are more vulnerable to hydraulic failure, which had lower mean iWUE (38–40). Mean iWUE was also different among trees with different leaf types, with needleleaf evergreen trees being the highest, followed by needleleaf deciduous trees, broadleaf evergreen trees, and finally broadleaf deciduous trees (SI Appendix, Fig. S4D).

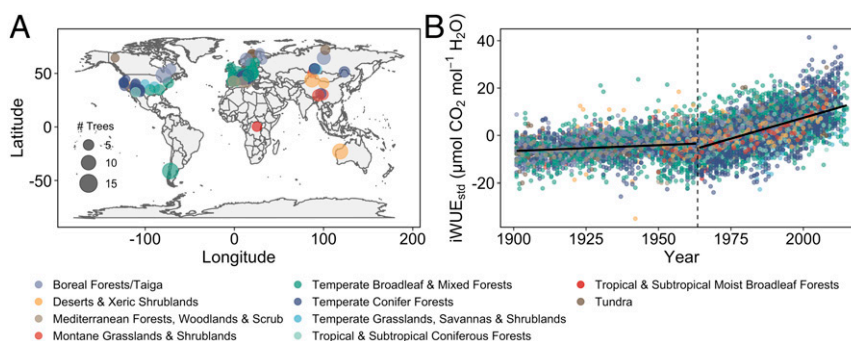


Fig. 1. Tree locations from which chronologies of iWUE and $\Delta^{18}\text{O}_{\text{lw}}$ were developed (A) and group mean-centered iWUE by species within site over the period 1901–2015 (B). The color of data points in A and B correspond to the biome from which trees were growing, while the size of the circle in A corresponds to the number of trees used in the development of each carbon and oxygen isotope-derived chronology, respectively. The vertical dashed line in B occurs at the year 1963 where the rate of change in iWUE increases. The solid lines in B denote the average trend in iWUE for the period before (1901–1963) and after (1963–2015) the identified breakpoint. Data for iWUE trends and the number of trees per chronology are listed in SI Appendix, Table S1.

Changes in climate and C_a have strong effects on vegetation function from the leaf (14, 15) to global scale (13, 41, 42), yet how environmental change has influenced iWUE across large spatial scales over the last century is not fully resolved. Guerrieri et al. (9) and Frank et al. (6) recently showed increasing C_a and climate change have led to increased iWUE in tree species across the United States and Europe, but whether this response is conserved across biomes experiencing a much larger range in climate is still unknown. To address this knowledge gap, we used linear mixed effects (LME) models to examine the importance of environmental factors in driving tree iWUE. Across all species and study locations from 1963–2015, LME model results explained as much as ~89% of the variance in iWUE and indicated a strong, positive relationship with C_a and growing season vapor pressure deficit (VPD_{grw}) and a negative relationship with growing season precipitation (PPT_{grw}), although a large proportion of the total variance was attributed to differences among sites (Table 1 and *SI Appendix, Table S3*). Remaining unaccounted variance may include non-climatic factors, such as nitrogen availability or acidic air pollution, which are known to have important influences over iWUE (19, 43, 44), but these were not included in the studies from which we extracted isotopic data. When extending this analysis to changes in iWUE over the last 115 y (1901–2015), LME model main effects were remarkably consistent with data from 1963–2015, with the exception of growing season temperature (TMP_{grw}) having a marginally positive effect on iWUE across the 115-y chronology (*SI Appendix, Table S4*), which suggests TMP_{grw} is becoming more important in recent years.

As a complement to our analysis using LME models to examine the effects of C_a , PPT_{grw} , TMP_{grw} , and VPD_{grw} on tree iWUE, we used hierarchical partitioning (HP), which alleviates potential problems that arise due to multicollinearity, to estimate the individual contribution of a given environmental parameter to tree iWUE. For the period 1901–2015, HP indicated that, of the 42% variance in iWUE explained by our model, C_a accounted for 59.6% ($z = 1,375.5$, $P < 0.05$), more than any other factor considered. We

found VPD_{grw} , TMP_{grw} , and PPT_{grw} contributed 23.6% ($z = 501.3$, $P < 0.05$), 16.2% ($z = 340.1$, $P < 0.05$), and 0.6% ($z = 12.6$, $P < 0.05$), respectively. Of the 31% variance in iWUE explained in our model over the period 1963–2015, the influence of C_a declined to 45.2% ($z = 455.6$, $P < 0.05$), consistent with Adams et al. (32), who found a diminishing rate of response of iWUE to CO_2 after 1966 (*SI Appendix, Fig. S5*). On the other hand, the influence of TMP_{grw} increased to 28.0% ($z = 357.2$, $P < 0.05$), whereas the contributions of VPD_{grw} and PPT_{grw} were similar to the 1963–2015 chronology with 26.1% ($z = 269.7$, $P < 0.05$) and 0.7% ($z = 6.4$, $P < 0.05$), respectively.

Increasing C_a may affect both stomatal conductance and photosynthesis (14, 15). VPD, or dryness of the atmosphere, regulates stomatal conductance (45), and therefore, both photosynthesis and transpiration (46). Air temperature drives VPD (46), but also affects leaf metabolism, including the ratio of photosynthesis to photorespiration (47). Precipitation is a proxy for soil moisture content and, thus, the amount of water available for uptake by plant roots. Thus, the individual effects of C_a , VPD_{grw} , PPT_{grw} , and TMP_{grw} on our observations of iWUE over the last 115 y are grounded in well-established plant physiology (6, 7, 48, 49). Here, we show that these environmental drivers interact to regulate tree iWUE and are dependent on leaf and wood functional types, demonstrating the complexity and nuance of tree responses to environmental change. In many instances, the effects of increasing C_a were modulated either positively or negatively by the other drivers of iWUE and by leaf and wood functional types. There was a C_a by VPD_{grw} interaction across the 115-y chronology (*SI Appendix, Fig. S6A*) and when considering only the chronology after the 1963 breakpoint (Fig. 24), whereby VPD_{grw} had a greater effect on iWUE at lower C_a than at higher C_a and the effect of increasing C_a on iWUE was diminished by greater VPD_{grw} . This may, in part, explain the diminishing influence of C_a on iWUE presented by Adams et al. (32) in recent years if VPD_{grw} has also been increasing at the study locations. In contrast, the effect of C_a

Table 1. LME model results and parameters for the best model (lowest AICc) examining the drivers of tree ring-derived iWUE for the period 1963–2015

Parameter	1963–2015	1963–2015 _{wood}	1963–2015 _{leaf}
Intercept, $\mu\text{mol}\cdot\text{mol}^{-1}$	83.078 \pm 1.401***	87.297 \pm 1.292***	87.592 \pm 1.326***
C_a , ppm	0.238 \pm 0.007***	0.238 \pm 0.007***	0.238 \pm 0.007***
PPT_{grw} , mm	−0.010 \pm 0.001***	−0.010 \pm 0.001***	−0.010 \pm 0.001***
TMP_{grw} , °C	0.246 \pm 0.135 ^{ns}	0.245 \pm 0.135 ^{ns}	0.245 \pm 0.135 ^{ns}
VPD_{grw} , kPa	13.141 \pm 1.476***	13.131 \pm 1.477***	13.131 \pm 1.477***
CO_2 : TMP_{grw}	0.012 \pm 0.007 ^{ns}	0.012 \pm 0.007 ^{ns}	0.012 \pm 0.007 ^{ns}
CO_2 : VPD_{grw}	−0.175 \pm 0.073*	−0.172 \pm 0.073*	−0.172 \pm 0.073*
TMP_{grw} : VPD_{grw}	1.919 \pm 0.915*	—	1.936 \pm 0.915*
Diffuse porous	—	−17.641 \pm 2.851***	—
Ring porous	—	−18.321 \pm 2.727***	—
Needleleaf deciduous	—	—	−3.064 \pm 2.667 ^{ns}
Broadleaf evergreen	—	—	−10.720 \pm 7.954 ^{ns}
Broadleaf deciduous	—	—	−18.952 \pm 2.285***
Marginal R^2	0.12	0.38	0.39
Conditional R^2	0.88	0.89	0.89

LME model results and parameters for the best model (lowest AICc) examining the drivers of tree ring-derived iWUE for the period 1963–2015 when only considering environmental factors, climate, and CO_2 (second column), including wood type as a fixed effect with no interactions in the model (third column), and when including leaf type as a fixed effect with no interactions in the model (fourth column). Intercept values for each model represent the value of iWUE when each numerical environmental factor included in the model is at its mean value during the study period. Leaf and wood type parameter estimates indicate the difference from the original intercept value for each respective variable, with comparisons made with “conifers” at the base level for wood type and “needleleaf evergreen” as the base level for leaf type. The marginal R^2 describes the goodness of model fit given fixed effects only, while the conditional R^2 describes the goodness of model fit including fixed and random effects (tree species nested within site). Model parameter significance is denoted by an asterisk, where * $P < 0.05$, ** $P < 0.01$, and *** $P < 0.001$, and “ns” denotes not significant.

on iWUE was enhanced at greater temperatures across the 115-y chronology (SI Appendix, Fig. S6B).

Furthermore, we found increasing C_a led to greater increases in iWUE in conifer trees, with respect to trees that had diffuse porous or ring porous wood, and the effect of C_a was diminished in broadleaf deciduous trees relative to needleleaf evergreen trees (SI Appendix, Table S3). When considering leaf type, we found that C_a interacted with PPT_{grw} where the effects of increasing C_a on iWUE were greatest with low PPT_{grw} and diminished at high PPT_{grw} for needleleaf evergreen (Fig. 3A) and needleleaf deciduous (Fig. 3B), in contrast to broadleaf deciduous trees where the effect of increasing C_a offset the negative effects of high PPT_{grw} on iWUE (Fig. 3C). These results suggest that iWUE of broadleaf deciduous trees may remain high as C_a continues to increase regardless of PPT_{grw} , whereas high PPT_{grw} offsets the C_a response of iWUE in conifers, which are adapted to drier environments (50). We found no interaction between C_a and PPT_{grw} on iWUE of broadleaf evergreen trees, which instead showed an interaction between C_a and VPD_{grw} on iWUE (Fig. 3D). In other instances, the effects of air temperature were modulated by either VPD_{grw} or precipitation. The response of tree iWUE to TMP_{grw} after 1963 was dependent upon VPD_{grw} (Table 1), such that the effect of TMP_{grw} on iWUE was the greatest at high VPD_{grw} (Fig. 2B). We found more complex interactions between TMP_{grw} and PPT_{grw} on iWUE when considering wood functional types, whereby the greatest iWUE for conifer tree species was at low PPT_{grw} and low TMP_{grw} (SI Appendix, Fig. S7A), but at low PPT_{grw} and high TMP_{grw} for diffuse porous trees (SI Appendix, Fig. S7B). On the other hand, ring porous trees showed an interaction between VPD_{grw} and PPT_{grw} , where iWUE was greatest at low PPT_{grw} and high VPD_{grw} (SI Appendix, Fig. S7C). Thus, these interactive effects are important to understand as they underscore the intricate interplay between C_a , temperature, precipitation, and evaporative water demand on tree physiology, highlight important differences in tree responses to environmental change across tree functional traits, and have important implications for tree carbon gain and water loss as climate changes and C_a continues to rise (46, 49).

Annually resolved, canopy-integrated iWUE chronologies reconstructed from tree ring carbon isotope signatures clearly show a positive trend over the 20th century explained, in part, by interactions between C_a , PPT_{grw} , VPD_{grw} , and TMP_{grw} . However, whether the increases in iWUE were due to underlying stimulated A_{net} , reduced g_s , or some combination thereof, cannot be explained using carbon isotope signatures alone. Therefore, we combined analyses of the chronologies of iWUE with those of $\Delta^{18}O_{lw}$ (which is inversely related to g_s) to partition the increases in iWUE between independent changes in A_{net} and g_s . Of all chronologies showing an increase in iWUE since 1963 (Fig. 4A–C), we found 5.3% ($n = 6$) of the studies showed decreasing $\Delta^{18}O_{lw}$ (Fig. 4D), indicating increased g_s across the 53-y period; 77.9% ($n = 88$) showed constant

$\Delta^{18}O_{lw}$ (Fig. 4E), indicating no significant change in g_s ; and 16.8% ($n = 19$) showed increasing $\Delta^{18}O_{lw}$ (Fig. 4F), reflecting a decrease in g_s (22, 23, 25, 30, 51). Trends in $\Delta^{18}O_{lw}$ over time were not different among wood types ($F = 1.39$, $P = 0.25$) (SI Appendix, Fig. S8A), although there were differences due to leaf type ($F = 4.60$, $P = 0.03$), with broadleaf deciduous trees showing slightly increasing $\Delta^{18}O_{lw}$, corresponding to a decrease in g_s , but all other leaf types being no different from each other and having either a nonsignificant slope or a negative slope (SI Appendix, Fig. S8B). There were no relationships between individual trends in $\Delta^{18}O_{lw}$ and mean TMP_{grw} and mean PPT_{grw} across all chronologies since 1963 (SI Appendix, Fig. S9A and B), nor was there a relationship between individual trends in $\Delta^{18}O_{lw}$ and individual trends in TMP_{grw} (SI Appendix, Fig. S9D). Mean $\Delta^{18}O_{lw}$, however, did decrease with increasing mean VPD_{grw} , although this relationship was overwhelmingly driven by a few sites ($n = 5$) (SI Appendix, Fig. S9C). Finally, trends in $\Delta^{18}O_{lw}$ tended to become more negative, corresponding to increased g_s , in sites becoming wetter since 1963 (SI Appendix, Fig. S9E) and more positive, corresponding to reduced g_s , in sites where VPD was increasing (SI Appendix, Fig. S9F), although the variability in $\Delta^{18}O_{lw}$ trends explained by PPT_{grw} trends and VPD_{grw} trends was only 9% and 8%, respectively. Analysis of the annual variability in $\Delta^{18}O_{lw}$ for each of the 113 chronologies since 1963 showed a positive relationship with VPD_{grw} (SI Appendix, Fig. S10) and TMP_{grw} (SI Appendix, Fig. S11), but a negative relationship with PPT_{grw} (SI Appendix, Fig. S12). Our findings are similar to Guerrieri et al. (9) who showed negative or constant $\Delta^{18}O_{lw}$ trends in wetter sites (increased or constant g_s , respectively) and align in magnitude and direction with the relationship between VPD and tree ring $\delta^{18}O$ presented for tropical trees by Kahmen et al. (52). Our analysis of $\Delta^{18}O_{lw}$ assumed 1) the oxygen isotopic composition of tree source water reflects that of precipitation, and 2) 40% of oxygen atoms exchange with stem water during cellulose synthesis ($p_{ex} = 0.40$) (53). We performed two sensitivity analyses to explore these assumptions, first by allowing a partial decoupling of precipitation and source water oxygen isotope composition, and second by changing p_{ex} across a range from 0.20 to 0.60, or by a climate-dependent value using the equation provided by Cheesman and Cernusak (54) derived from eucalypts in Northeast Tasmania and found that our overall conclusions using $p_{ex} = 0.4$ are highly robust (Methods and SI Appendix, Figs. S13–S17 and Table S5).

Whether the increases in tree iWUE are caused by increases in A_{net} , reductions in g_s , or a combination of changes in A_{net} or g_s are consequential as changes in A_{net} may affect the carbon cycle possibly through tree growth and carbon sequestration, while changes in g_s may affect the hydrologic cycle through changes in evapotranspiration. Our temporal analysis of trends in g_s inferred from individual $\Delta^{18}O_{lw}$ chronologies from 1963 to 2015 indicates that g_s increased in 5.3% of examined cases (Fig. 4D) and remained constant in 77.9% (Fig. 4E). Thus, it is necessary that

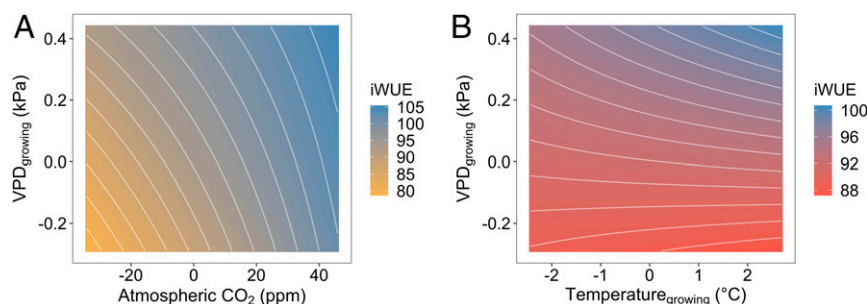


Fig. 2. Nature of the interaction between growing season vapor pressure deficit (VPD) and atmospheric CO₂ (A) and growing season VPD and growing season temperature (B) on iWUE during the period 1963–2015. The interactions shown represent a given predicted value of iWUE throughout the range experienced by each group mean-centered environmental factor since 1963. Values listed for each environmental factor are standardized with respect to the mean during the study period. Parameter estimates for each interaction are listed in Table 1.

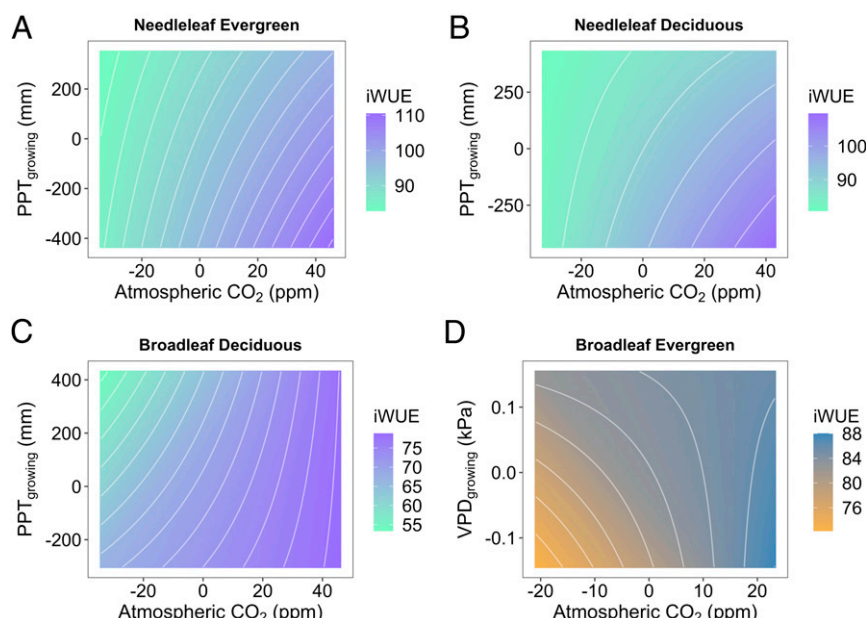


Fig. 3. Nature of the interaction between atmospheric CO₂ and growing season precipitation (PPT_{growing}) on iWUE for needleleaf evergreen (A), needleleaf deciduous (B), and broadleaf deciduous (C) tree species, and between atmospheric CO₂ and growing season VPD (VPD_{growing}) for broadleaf evergreen trees (D). The interactions shown represent a given predicted value of iWUE throughout the range experienced by each group mean-centered environmental factor since 1963. Values listed for each environmental factor are standardized with respect to the mean during the study period.

A_{net} had to increase in 83.2% of examined chronologies (i.e., sum of 5.3% and 77.9%) for iWUE to increase over the 53-y period. In the remaining 16.8% of the chronologies, g_s declined (Fig. 4F), and as such, increases in iWUE could have occurred because of reductions in g_s alone or in combination with increasing A_{net} (Fig. 4C and F). The widespread historical increase in A_{net} driving increases in tree iWUE was a surprising result to us since declines in g_s , and a consequent increase in iWUE, are common results found in elevated C_a experiments (14, 15, 55, 56). However, elevated C_a studies often rely on large step increases in C_a , whereas tree rings record responses to long-term progressive, but small, increases in C_a . Furthermore, analyses of g_s responses to increased C_a in trees indicate a large amount of variability with older trees showing less sensitivity than younger trees and conifers being less sensitive than deciduous trees (55). Indeed, ~70% of the chronologies in this study that showed decreasing g_s were broadleaf deciduous tree species. Our data using tree ring isotopes provide strong support of studies using carbonyl sulfide (13, 42, 57), satellite data (58), and seasonal C_a patterns (59) that show global increases in A_{net} as a result of increasing C_a (13, 42), and build upon recent observations showing widespread stimulated A_{net} resulting in increased iWUE in the United States (9). Moreover, the rates at which iWUE increased were highest in those chronologies with reduced g_s (Fig. 4C), followed by those with constant g_s (Fig. 4B), and the lowest in those chronologies with increased g_s (Fig. 4A). This highlights the importance of stimulated A_{net} in driving increasing iWUE in all cases, and supports reductions in g_s , inferred through increasing $\Delta^{18}\text{O}_{\text{lw}}$, exacerbating realized increases in iWUE in a small subset of chronologies. Finally, for those tree ring chronologies where no trends in iWUE were observed since 1963 ($n = 18$), the overwhelming majority of associated $\Delta^{18}\text{O}_{\text{lw}}$ chronologies were either constant ($n = 16$) or decreased ($n = 1$), suggesting any increases in A_{net} that may have occurred over the 53-y time period were not sufficient to offset the increase or constant g_s .

Our meta-analysis using historical $\Delta^{13}\text{C}$ and $\Delta^{18}\text{O}_{\text{lw}}$ from tree ring chronologies representing 34 species across 10 biomes establishes a strong process-based framework for predicting changes to tree iWUE across biomes and across wood and leaf functional types. It

further provides an extensive annual record documenting a ~40% increase in tree iWUE globally over the 20th century (Fig. 1), similar in magnitude to the ~34% increase in C_a that occurred over the same time (31). The rate at which iWUE increased more than tripled after 1963 and occurred within years of a similar breakpoint in C_a (SI Appendix, Fig. S2). Generally, C_a stimulated the rate of increased iWUE of conifers, which comprised ~74% of the examined chronologies, to a greater degree than trees with other wood anatomy. We identified increasing C_a as a main factor in driving increases in iWUE, although both C_a and TMP_{grw} interacted with other environmental drivers of iWUE in ways that suggest trees in areas that experience future increases in PPT_{grw} or reductions VPD_{grw} may have lower realized iWUE than those areas experiencing drier conditions or higher evaporative demand (Table 1). Metadata on leaf area index (6), tree level photosynthesis or hydraulic conductivity with age (60, 61), height or size effects on carbon isotope discrimination (62), or the levels of air pollution (19, 24, 63) were not consistently available from the published studies used in our analyses, and thus we cannot exclude potential effects of these factors on historical tree iWUE variance.

Coupling iWUE with $\Delta^{18}\text{O}_{\text{lw}}$ chronologies revealed increases in A_{net} as a consistent driver behind increasing iWUE across ~83% of the examined chronologies, while reduced g_s , or a combination of increasing A_{net} and reduced g_s , was responsible for increases in iWUE in the remaining ~17% (Fig. 4). The widespread patterns of stimulated A_{net} from this study are in line with recent findings of a 31% increase in global photosynthetic carbon gain over the 20th century (42), directly tracking increasing C_a (13, 42). Thus, this meta-analysis showing increased iWUE over the 20th century encompassing a spectrum of tree functional types across a broad geographic area highlights the complexity of tree responses to environmental change and reinforces the importance of stimulated photosynthesis, and not reductions in leaf g_s , as the primary driver in global increases in iWUE. These results provide a historical baseline of the environmental drivers and physiological mechanisms that result in the uptake of ~30% of anthropogenic carbon emissions by terrestrial ecosystems each year (64).

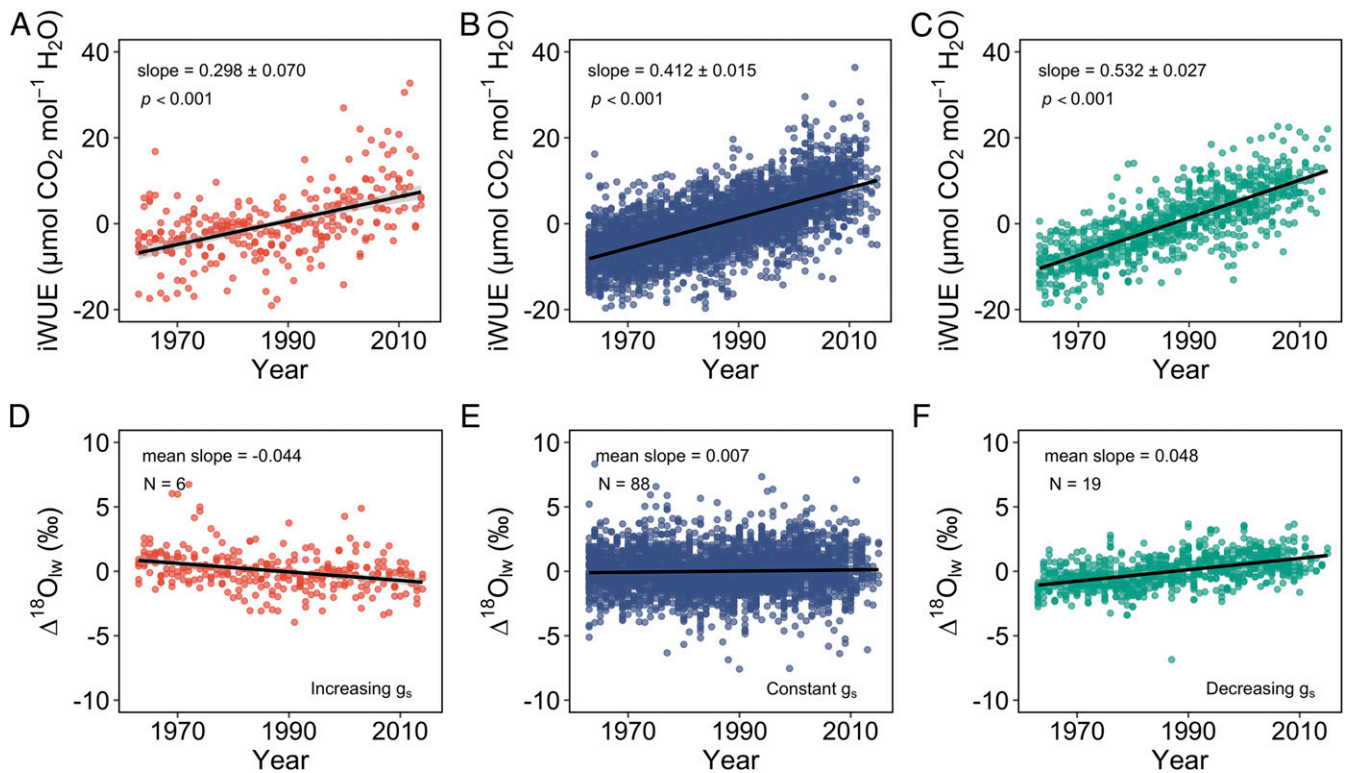


Fig. 4. Standardized chronologies of iWUE (A–C) and $\Delta^{18}\text{O}_{\text{lw}}$ (D–F) binned by the individual $\Delta^{18}\text{O}_{\text{lw}}$ trend for each chronology for the period 1963–2015. Red data points (A and D) contain individual chronologies with decreasing $\Delta^{18}\text{O}_{\text{lw}}$, blue data points (B and E) contain individual chronologies with constant $\Delta^{18}\text{O}_{\text{lw}}$, and green data points (C and F) contain individual chronologies with increasing $\Delta^{18}\text{O}_{\text{lw}}$. The respective slope for iWUE across all chronologies within each $\Delta^{18}\text{O}_{\text{lw}}$ category (decreasing, constant, increasing $\Delta^{18}\text{O}_{\text{lw}}$) is listed within each respective panel, along with the P value with the corresponding LME model fit where species chronology is nested within site as a random factor (see *SI Appendix, Table S1* for site chronologies). The mean slope across all $\Delta^{18}\text{O}_{\text{lw}}$ chronologies (N) within a given category is listed in the *Top Left* of each panel (D–F). The solid black line in each panel represents the average trend across all data points.

Materials and Methods

Data Collection and Extraction. Data were collected from published articles resulting from a literature search on Web of Science using the search phrase “tree ring, carbon, oxygen, isotope.” Articles published prior to the search date (July 15, 2019) were identified for potential use in our global analysis, and of the 378 candidate articles resulting from the search, 49 met all selection criteria for inclusion, which were as follows: 1) present raw, uncorrected $\delta^{13}\text{C}$ or $\delta^{13}\text{C}$ -derived variables (i.e., $\delta^{13}\text{C}$, iWUE) and $\delta^{18}\text{O}$ stable isotope signatures from absolutely dated tree ring chronologies, 2) provide identification information regarding tree species sampled and the respective tree ages, 3) include geographic coordinates of each study location, 4) contain high-quality figures from which the isotope data could be extracted or be accompanied by a publicly available supplemental data file, 5) contain metadata regarding the type of tree ring sample used (i.e., α -cellulose, bulk wood), and 6) be sampled from mature trees (>50 y) that were not subject to experimental treatments. Our literature search yielded 113 tree ring carbon and oxygen isotope chronologies comprising 36 tree species at 84 sites across the globe (*SI Appendix, Table S1*). Of these 113 chronologies, 84 were conifer tree species and 29 were deciduous tree species, and all but 3 chronologies were from the Northern Hemisphere.

We used WebPlotDigitizer, a data extraction application with built-in tools to extract data from a variety of plot types, with the ability to save files in TAR or JSON format (65), to retrieve $\delta^{13}\text{C}$ -derived and $\delta^{18}\text{O}$ isotope data from published figures. We first validated the accuracy and precision of extracted data using figures from our own previously published manuscripts (linear regression, $R^2 = 1.0$; slope = 1.0004; y-intercept = 0.001; $P < 0.001$). Then, from each article that met the selection criteria, we captured a high-quality image file for each relevant figure in TIFF format and assigned numerical values to the x axis and y axis, respectively. This was accomplished by assigning values to the known endpoints of each axis, in turn, and linearly interpolating values between the points. We then identified each unique data point on a given figure, after which the abscissa and ordinate were

automatically calculated. This was performed for each tree- or species-specific chronology within a given site. Typically, species-averaged chronologies for $\delta^{13}\text{C}$ -derived and $\delta^{18}\text{O}$ isotope data of all sampled trees were presented in published literature; however, in cases where individual tree chronologies were presented, we first extracted data for each year at the tree level before calculating a species-level mean for a given species within a given site, for direct comparison among observations across all studies.

Environmental factors examined as potential drivers of tree physiology in this study include atmospheric CO_2 (C_a , in parts per million), as well as climate factors temperature (TMP, in degrees Celsius), precipitation (PPT, in millimeters), and VPD (in kilopascals) given their relevance to large-scale controls over the carbon and hydrologic cycles (13, 49, 66, 67). Annual C_a concentrations were obtained from the Scripps Institution of Oceanography ice-core merged data product (31, 68), while climate data were obtained from the Climatic Research Unit (CRU TS4.03) global gridded data product (69). Climate data from the CRU TS4.03 data product were provided at a $0.5^\circ \times 0.5^\circ$ spatial resolution at monthly time step from 1901 to 2018 and were validated using local observations from ground-based meteorological stations. From the CRU TS4.03, we extracted TMP, PPT, and vapor pressure (VAP) (in hectopascals) for each of the 84 unique study locations, and calculated VPD from VAP and TMP using methods from Allen (70). We calculated annual (X_{ann}) and growing season (X_{grw}) values for each climate variable over the period 1901–2015 using means for TMP and VPD, while using sums for PPT. The range of months over which the growing season occurs is dependent upon the geographical site location and was determined based on information provided in each published article.

Last, we compiled characteristics unique to each site and chronology included in this analysis such as biome type, tree ring type, and tree phenology type (*SI Appendix, Table S1*). Biome type was determined based on GPS coordinates provided for each unique site coupled with a global geographical biome classification database outlined in Dinerstein et al. (71),

while tree ring type was determined based upon known ring anatomy confirmed using The Xylem Database (72).

Carbon Isotope Calculations. The extracted $\delta^{13}\text{C}$ -derived chronologies fell into four distinct categories—raw tree ring $\delta^{13}\text{C}$ ($\delta^{13}\text{C}_{\text{raw}}$, $n = 45$), atmospheric CO_2 -corrected $\delta^{13}\text{C}$ ($\delta^{13}\text{C}_{\text{cor}}$, $n = 36$), carbon isotope discrimination ($\Delta^{13}\text{C}$, $n = 25$), and iWUE ($n = 7$). While there is a consistent postphotosynthetic fractionation ($\sim 2\%$) between leaf organic matter and carbon assimilated into woody biomass (6, 73, 74), in addition to fractionation related to photorespiration (75), none of the published studies identified in our analysis took this into account when presenting values of $\delta^{13}\text{C}_{\text{cor}}$, $\Delta^{13}\text{C}$, or iWUE. As such, all published values of $\delta^{13}\text{C}_{\text{cor}}$, $\Delta^{13}\text{C}$, and iWUE were first converted to $\delta^{13}\text{C}_{\text{raw}}$ before calculation of $\delta^{13}\text{C}$ -derived chronologies that included these effects following Laverne et al. (76). We calculated $\delta^{13}\text{C}_{\text{raw}}$ when values of atmospheric $\delta^{13}\text{C}$ -corrected $\delta^{13}\text{C}$ were given using the following:

$$\delta^{13}\text{C}_{\text{raw}} = \delta^{13}\text{C}_{\text{cor}} + (\delta^{13}\text{C}_{\text{atm}} + 6.4), \quad [1]$$

and when discrimination, $\Delta^{13}\text{C}$, was presented using the following:

$$\delta^{13}\text{C}_{\text{raw}} = \frac{1,000 * \Delta^{13}\text{C} - 1,000 * \delta^{13}\text{C}_{\text{atm}}}{1,000 + \Delta^{13}\text{C}}, \quad [2]$$

where $\delta^{13}\text{C}_{\text{atm}}$ is the carbon isotopic signature of atmospheric CO_2 on the year of ring formation ($\sim 6.4\%$ being the $\delta^{13}\text{C}_{\text{atm}}$ signature prior to the industrial revolution) (77, 78). For all calculations during the period 1901–2003, we used McCarroll and Loader (78) for $\delta^{13}\text{C}_{\text{atm}}$ values. Beyond 2003, $\delta^{13}\text{C}_{\text{atm}}$ values were calculated linearly extrapolating the trend beginning at the 1962 $\delta^{13}\text{C}_{\text{atm}}$ breakpoint. In cases where iWUE was presented, we first calculated $\Delta^{13}\text{C}$ using the following:

$$\Delta^{13}\text{C} = \frac{\frac{-\text{iWUE}}{0.625} * (b - a) + C_a * (b - a)}{C_a}, \quad [3]$$

where a (4.4‰) is the fractionation associated with the diffusion of CO_2 (77, 79), b (28‰) is the mean fractionation related to the preferential utilization of $^{12}\text{CO}_2$ over $^{13}\text{CO}_2$ during carboxylation by Rubisco (75, 77), and C_a is the atmospheric CO_2 concentration during the year of ring formation (31, 68). We then used Eq. 2 to calculate $\delta^{13}\text{C}_{\text{raw}}$ from $\Delta^{13}\text{C}$ (77, 80). To calculate iWUE from $\delta^{13}\text{C}_{\text{raw}}$ including photorespiration and postphotosynthetic fractionation effects, we first calculated leaf internal CO_2 (C_i) using the following:

$$C_i = \frac{\left(\frac{\delta^{13}\text{C}_{\text{atm}} - (\delta^{13}\text{C}_p - d)}{1 + \frac{(\delta^{13}\text{C}_p - d)}{1,000}} \right) - a - f * \left(\frac{1}{p_{\text{CO}_2}} \right)}{b - a} * C_a, \quad [4]$$

where $\delta^{13}\text{C}_p$ is the isotopic signature of the tree ring, d accounts for the carbon isotope fractionation from leaf to wood (bulk wood = 1.9‰; cellulose = 2.1‰) (6, 73), f is the isotopic fractionation associated with photorespiration (12‰) (75), p_{CO_2} is the partial pressure of atmospheric CO_2 (in pascals), and Γ^* is the CO_2 compensation point in the absence of dark respiration (in pascals) (76). We calculated Γ^* according to the following:

$$\Gamma^* = \Gamma_{25}^* * \left(\frac{P_{\text{atm}}}{P_0} \right) * e^{\left(\frac{\Delta H_a}{RT} * \left(\frac{1}{298} - \frac{1}{T} \right) \right)}, \quad [5]$$

where ΔH_a is the energy of activation (37,830 J·mol $^{-1}$) (81), T is the leaf temperature (in degrees Celsius), R is the molar gas constant (8.314 J·mol $^{-1}$ ·K), P_{atm} is the ambient atmospheric pressure (in pascals), P_0 is the atmospheric pressure at sea level (101,325 Pa), and Γ_{25}^* is the CO_2 compensation point at 25 °C (4.332 Pa) (81, 82). We assumed T reflects the mean air temperature over the growing season. We then calculated iWUE (in micromoles of CO_2 ·moles $^{-1}$ H_2O) as follows:

$$\text{iWUE} = \frac{(C_a - C_i)}{1.6}, \quad [6]$$

where 1.6 is the constant ratio for the diffusivity of water vapor and CO_2 in air. For each of the preceding calculations, we assumed leaf structure, mesophyll conductance (g_m), and mesophyll CO_2 fractionation remained unchanged throughout the length of each of the chronologies (83); however, we do realize minor species differences in leaf morphology or small changes over time due to environmental influences could have minor influences over g_m , and thus $\delta^{13}\text{C}$ -derived chronologies (84). Although it could increase uncertainty around our estimates of C_i , and thus iWUE, this assumption is

nevertheless standard across dendroisotopic studies reconstructing iWUE from tree ring carbon isotopes (6, 8, 9, 18, 19, 76).

Oxygen Isotope Calculations. We calculated tree ring ^{18}O enrichment above the source water ($\Delta^{18}\text{O}_{\text{tr}}$) from raw tree ring $\delta^{18}\text{O}$ ($\delta^{18}\text{O}_{\text{tr}}$) using the following:

$$\Delta^{18}\text{O}_{\text{tr}} = \frac{\delta^{18}\text{O}_{\text{tr}} - \delta^{18}\text{O}_p}{1 + \left(\frac{\delta^{18}\text{O}_p}{1,000} \right)}, \quad [7]$$

where $\delta^{18}\text{O}_p$ is the oxygen isotopic composition of precipitation during ring formation (54). Given the lack of long-term records of $\delta^{18}\text{O}_p$ at the study locations, we estimated site-specific $\delta^{18}\text{O}_p$ over the length of each respective chronology following methods from Guerrieri et al. (9) using the following:

$$\delta^{18}\text{O}_p = 0.52 * T_a - 0.006 * T_a^2 + 2.42 * P_a - 1.43 * P_a^2 - 0.046 * \sqrt{E} - 13, \quad [8]$$

where T_a is the mean annual temperature (in degrees Celsius), P_a is total annual precipitation (in meters), and E is the elevation (in meters) of the study location above sea level (85) (SI Appendix, Fig. S18). We used linear regression to validate our estimated values of $\delta^{18}\text{O}_p$ using Eq. 8 against those obtained from isoMAP (86) for the period 1985–2015 ($R^2 = 0.94$, $P < 0.01$) (SI Appendix, Fig. S19). Finally, from $\Delta^{18}\text{O}_{\text{tr}}$ we calculated the enrichment of leaf water ^{18}O above source water ($\Delta^{18}\text{O}_{\text{lw}}$) using the following:

$$\Delta^{18}\text{O}_{\text{lw}} = \frac{\Delta^{18}\text{O}_{\text{tr}} - \varepsilon_{\text{wc}}}{1 - p_{\text{ex}}}, \quad [9]$$

where ε_{wc} is the temperature-dependent fractionation associated with carbonyl oxygen atoms exchanging with water during wood (i.e., cellulose) synthesis (54, 87) and p_{ex} is the fraction of stem water at the site of cellulose synthesis, of which a given proportion of oxygen atoms, p_{ex} , are exchanged. We calculated ε_{wc} following Sternberg and Ellsworth (53) using the following:

$$\varepsilon_{\text{wc}} = 0.0084 * T_a^2 - 0.51 * T_a + 33.172, \quad [10]$$

while $p_{\text{ex}} \sim 1$, a value in the range of 0.20 to 0.42, is typically used for p_{ex} (27, 53, 88), with higher values of p_{ex} often observed in more arid sites (54). For this study, we used a conservative value (0.40) for p_{ex} (53), although we acknowledge p_{ex} may differ across sites with different climates (54). Thus, we performed two sensitivity analyses to examine how changes in p_{ex} subsequently influenced $\Delta^{18}\text{O}_{\text{lw}}$ described in greater detail below. Trends in calculated values of $\Delta^{18}\text{O}_{\text{lw}}$ were then used to infer changes in g_s for each individual chronology based on well-established physiological theory describing the inverse relationship between $\Delta^{18}\text{O}_{\text{lw}}$ and g_s (i.e., increasing $\Delta^{18}\text{O}_{\text{lw}}$ indicates reductions in g_s and decreasing $\Delta^{18}\text{O}_{\text{lw}}$ indicates increasing g_s , while constant $\Delta^{18}\text{O}_{\text{lw}}$ indicates no significant change in g_s) (26–30).

One caveat when interpreting $\Delta^{18}\text{O}_{\text{lw}}$ calculated from tree rings is that in some cases the environmental signal can be muted (i.e., leaf and wood oxygen isotope signatures may become uncoupled) (89), potentially obscuring the inferred g_s , especially if precipitation $\delta^{18}\text{O}$ is decoupled from source water $\delta^{18}\text{O}$. We first addressed this issue by using ordinary least-squares regression to examine the relationship between calculated $\Delta^{18}\text{O}_{\text{lw}}$ and PPT $_{\text{grw}}$, VPD $_{\text{grw}}$, and TMP $_{\text{grw}}$ for each of the 113 unique chronologies used in this study (SI Appendix, Figs. S10–S12), which show a similar relationship between $\Delta^{18}\text{O}_{\text{lw}}$ and VPD $_{\text{grw}}$ with Kahmen et al. (52), who found a strong preservation of environmental signals in tree ring oxygen isotope composition. Furthermore, we conducted a sensitivity analysis to determine the degree to which precipitation $\delta^{18}\text{O}$ being uncoupled from source water $\delta^{18}\text{O}$ may influence our estimates of $\Delta^{18}\text{O}_{\text{lw}}$, the resulting long-term $\Delta^{18}\text{O}_{\text{lw}}$ trends, and the consequences for inferred changes in A_{net} and g_s , as iWUE increased (SI Appendix, Fig. S13 and Table S5). To do this, we used calculated values of $\delta^{18}\text{O}_p$ from Eq. 8 used in our analyses to generate simulated data for each chronology with a resulting Pearson's product-moment correlation with the actual $\delta^{18}\text{O}_p$ of 0.90, 0.80, 0.70, and 0.60, respectively. These scenarios, in turn, represent a 10%, 20%, 30%, and 40% decoupling of $\delta^{18}\text{O}$ source water from $\delta^{18}\text{O}_p$. We then used ANOVA and analysis of covariance (ANCOVA) to test whether uncoupling influenced mean $\Delta^{18}\text{O}_{\text{lw}}$, or the rate of change in $\Delta^{18}\text{O}_{\text{lw}}$ over time. Last, we binned the chronologies by whether they showed increasing, constant, or decreasing $\Delta^{18}\text{O}_{\text{lw}}$ as a consequence of uncoupling of $\delta^{18}\text{O}_p$ and source water $\delta^{18}\text{O}$ to examine the consequences for our main conclusions regarding changes in A_{net} and g_s (SI Appendix, Table S5).

In addition to the potential for precipitation $\delta^{18}\text{O}$ to become uncoupled from source water $\delta^{18}\text{O}$, the proportion of oxygen exchanging with local water during cellulose synthesis (p_{ex}) may vary as a function of climate (54). Our second sensitivity analysis was designed to address how changes in p_{ex} influence $\Delta^{18}\text{O}_{\text{IW}}$ and the overall conclusions drawn from our dual isotope analysis (SI Appendix, Table S5). We performed this first by calculating $\Delta^{18}\text{O}_{\text{IW}}$ as a constant with $p_{\text{ex}} = 0.2, 0.4$, and 0.6 , and second where p_{ex} was allowed to vary as a function of mean annual precipitation, assuming the equation provided by Cheesman and Cernusak (54), derived from eucalypts in Northeast Tasmania, is consistent with values of p_{ex} of the chronologies for the sites used in our study (SI Appendix, Figs. S14 and S15). We used ANCOVA to test whether trends in $\Delta^{18}\text{O}_{\text{IW}}$ over time was dependent upon the value of p_{ex} used (SI Appendix, Fig. S16). We then used ordinary least-squares regression to examine the strength, and nature, of the relationship between $\Delta^{18}\text{O}_{\text{IW}}$ and VPD_{grw} for each p_{ex} scenario (SI Appendix, Fig. S17). Results for this analysis are described in the figure legends (SI Appendix, Figs. S14–S17), and these data led us to conclude that varying p_{ex} from 0.4 by a constant did not significantly affect the number of $\Delta^{18}\text{O}_{\text{IW}}$ trends that increased, decreased, or did not change over time. Varying p_{ex} by trying to account for different ecosystem climates resulted in four additional chronologies showing decreasing or constant $\Delta^{18}\text{O}_{\text{IW}}$ and reduced the number of chronologies showing increasing $\Delta^{18}\text{O}_{\text{IW}}$ by 8, but this did not change the overall conclusions of our study (SI Appendix, Table S5).

Statistical Analyses. To examine long-term trends in iWUE, we fit a LME model using the R package *nlme* (90) including *year* as the sole fixed effect with *tree species* nested within *site* as random factors. In this analysis, we examined trends in iWUE across the entire chronology for which climate data were available (full: 1901–2015), in addition to two unique periods (pre: 1901–1963; post: 1963–2015) after we identified a breakpoint in the full iWUE chronology (across all sites and species) using the *segmented* package in R (91). We further assessed breakpoints in individual chronologies, with the requirement there was a ± 25 -y buffer with respect to 1963 (SI Appendix, Fig. S1). Additionally, we used generalized least-squares (GLS) regression to examine trends in isotope-derived response variables (iWUE, $\Delta^{18}\text{O}_{\text{IW}}$, etc.) separately for each species within a given site, as well as for environmental factors (PPT, TMP, etc.) at a given site for each time period (i.e., full, pre, post) using the R package *nlme* (90). Each LME and GLS model used to determine temporal trends were fit via restricted maximum likelihood and included a first-order autocorrelation structure to account for temporal autocorrelation in the chronologies.

We further used LME models to identify which environmental factors were most responsible in driving the observed changes in iWUE over the last

115 y using the R package *nlme* (90). We used the *dredge()* function from the *MuMIn* R package (92) to examine all possible model LME model combinations ($n = 113$) that included the environmental factors C_a , TMP_{grw} , PPT_{grw} , VPD_{grw} , wood type, and leaf type as independent variables, as well as interactions up to order 2. We identified the top candidate model as having the lowest corrected Akaike information criterion (AIC_c) for subsequent parameter inference. Prior to this analysis continuous environmental factors were grouped by each unique chronology and centered to their mean to prevent issues that arise due to multicollinearity (9, 93). Each LME model examined included a temporal autocorrelation structure of order 1 [i.e., AR(1,0)], as well as species nested within site as a random factor, and were fit via maximum likelihood for comparison of models with different fixed effects. The top candidate model was then refit via restricted maximum likelihood. We used the R package *visreg* (94) to visualize the nature of significant interactions between environmental factors on iWUE over the range experienced by each factor.

As a complement to LME model parameter inference, we examined the independent effects of each environmental factor included as a fixed effect in the final model on iWUE through hierarchical partitioning (HP) using the R package *hier.part* (95). HP does not consider potential interactions between factors, but instead determines the contribution of a given environmental factor to iWUE through an examination of every possible model structure containing a given predictor variable. By doing so, HP avoids enhancing or diminishing the variance explained by any given predictor variable, and circumvents issues related to multicollinearity among predictor variables (96). To do this, we used the *rand.hp()* function, which randomizes the matrices containing response and predictor variables and computes independent effects, which we set at 1,000 repetitions to determine variable contributions to iWUE.

We performed ANCOVA to examine differences in the rate of change of iWUE and $\Delta^{18}\text{O}_{\text{IW}}$ over time that depended upon leaf type, wood type, or biome, and performed ANOVA to compare iWUE means between leaf type, wood type, and biome. Furthermore, we used the R package *emmeans* (97) to test for pairwise differences among groups from ANCOVA model fits, and used the R package *multcomp* (98) to generate connecting letters reports from Tukey's honestly significant difference post hoc test for multiple comparisons of means from ANOVA model fits.

Data Availability. All tree ring isotope data and code supporting this analysis have been deposited on Figshare (<https://doi.org/10.6084/m9.figshare.13541927>).

ACKNOWLEDGMENTS. We thank Drs. William Peterjohn, Edward Brzostek, David Nelson, and three anonymous reviewers for thoughtful and constructive comments on the manuscript. This research was funded by NSF Award 1354689.

- G. J. Kooperman et al., Plant physiological responses to rising CO_2 modify simulated daily runoff intensity with implications for global-scale flood risk assessment. *Geophys. Res. Lett.* **45**, 12,457–12,466 (2018).
- A. L. S. Swann, F. M. Hoffman, C. D. Koven, J. T. Randerson, Plant responses to increasing CO_2 reduce estimates of climate impacts on drought severity. *Proc. Natl. Acad. Sci. U.S.A.* **113**, 10019–10024 (2016).
- P. S. Nobel, *Physicochemical and Environmental Plant Physiology* (Academic, 1991).
- T. F. Keenan et al., Increase in forest water-use efficiency as atmospheric carbon dioxide concentrations rise. *Nature* **499**, 324–327 (2013).
- L. Lemondant, P. Gentine, A. S. Swann, B. I. Cook, J. Scheff, Critical impact of vegetation physiology on the continental hydrologic cycle in response to increasing CO_2 . *Proc. Natl. Acad. Sci. U.S.A.* **115**, 4093–4098 (2018).
- D. C. Frank et al., Water-use efficiency and transpiration across European forests during the Anthropocene. *Nat. Clim. Chang.* **5**, 579–583 (2015).
- P. van der Sleen et al., No growth stimulation of tropical trees by 150 years of CO_2 fertilization but water-use efficiency increased. *Nat. Geosci.* **8**, 24–28 (2015).
- J. Peñuelas, J. G. Canadell, R. Ogaya, Increased water-use efficiency during the 20th century did not translate into enhanced tree growth. *Glob. Ecol. Biogeogr.* **20**, 597–608 (2011).
- R. Guerrieri et al., Disentangling the role of photosynthesis and stomatal conductance on rising forest water-use efficiency. *Proc. Natl. Acad. Sci. U.S.A.* **116**, 16909–16914 (2019).
- J. Knauer et al., The response of ecosystem water-use efficiency to rising atmospheric CO_2 concentrations: Sensitivity and large-scale biogeochemical implications. *New Phytol.* **213**, 1654–1666 (2016).
- R. F. Keeling et al., Atmospheric evidence for a global secular increase in carbon isotopic discrimination of land photosynthesis. *Proc. Natl. Acad. Sci. U.S.A.* **114**, 10361–10366 (2017).
- A. Ito, M. Inatomi, Water-use efficiency of the terrestrial biosphere: A model analysis focusing on interactions between the global carbon and water cycles. *J. Hydrometeorol.* **13**, 681–694 (2012).
- L. A. Cernusak et al., Robust response of terrestrial plants to rising CO_2 . *Trends Plant Sci.* **24**, 578–586 (2019).
- E. A. Ainsworth, A. Rogers, The response of photosynthesis and stomatal conductance to rising $[\text{CO}_2]$: Mechanisms and environmental interactions. *Plant Cell Environ.* **30**, 258–270 (2007).
- E. A. Ainsworth, S. P. Long, What have we learned from 15 years of free-air CO_2 enrichment (FACE)? A meta-analytic review of the responses of photosynthesis, canopy properties and plant production to rising CO_2 . *New Phytol.* **165**, 351–371 (2005).
- P. J. Franks et al., Sensitivity of plants to changing atmospheric CO_2 concentration: From the geological past to the next century. *New Phytol.* **197**, 1077–1094 (2013).
- R. Rumman, O. K. Atkin, K. J. Bloomfield, D. Eamus, Variation in bulk-leaf ^{13}C discrimination, leaf traits and water-use efficiency-trait relationships along a continental-scale climate gradient in Australia. *Glob. Change Biol.* **24**, 1186–1200 (2018).
- R. B. Thomas, S. E. Spal, K. R. Smith, J. B. Nippert, Evidence of recovery of *Juniperus virginiana* trees from sulfur pollution after the Clean Air Act. *Proc. Natl. Acad. Sci. U.S.A.* **110**, 15319–15324 (2013).
- J. M. Mathias, R. B. Thomas, Disentangling the effects of acidic air pollution, atmospheric CO_2 , and climate change on recent growth of red spruce trees in the Central Appalachian Mountains. *Glob. Change Biol.* **24**, 3938–3953 (2018).
- G. Xu et al., Disentangling contributions of CO_2 concentration and climate to changes in intrinsic water-use efficiency in the arid boreal forest in China's Altay Mountains. *Forests* **9**, 642 (2018).
- T. M. Scanlon, D. F. Schmidt, T. H. Skaggs, Correlation-based flux partitioning of water vapor and carbon dioxide fluxes: Method simplification and estimation of canopy water use efficiency. *Agric. For. Meteorol.* **279**, 107732 (2019).
- Y. Scheidegger, M. Saurer, M. Bahn, R. Siegwolf, Linking stable oxygen and carbon isotopes with stomatal conductance and photosynthetic capacity: A conceptual model. *Oecologia* **125**, 350–357 (2000).
- T. E. E. Grams, A. R. Kozovits, K. H. Häberle, R. Matyssek, T. E. Dawson, Combining $\delta^{13}\text{C}$ and $\delta^{18}\text{O}$ analyses to unravel competition, CO_2 and O_3 effects on the physiological performance of different-aged trees. *Plant Cell Environ.* **30**, 1023–1034 (2007).
- T. Boettger, M. Haupt, M. Friedrich, J. S. Waterhouse, Reduced climate sensitivity of carbon, oxygen and hydrogen stable isotope ratios in tree-ring cellulose of silver fir (*Abies alba* Mill.) influenced by background SO_2 in Franconia (Germany, Central Europe). *Environ. Pollut.* **185**, 281–294 (2014).
- R. Bögelein, M. Hassdenteufel, F. M. Thomas, W. Werner, Comparison of leaf gas exchange and stable isotope signature of water-soluble compounds along canopy gradients of co-occurring Douglas-fir and European beech. *Plant Cell Environ.* **35**, 1245–1257 (2012).

26. G. D. Farquhar, J. Lloyd, "Carbon and oxygen isotope effects in the exchange of carbon dioxide between terrestrial plants and the atmosphere" in *Stable Isotopes and Plant Carbon-Water Relations*, J. R. Ehleringer, A. E. Hall, G. D. Farquhar, Eds. (Academic, San Diego, 1993), pp. 47–70.
27. L. A. Cernusak, G. D. Farquhar, J. S. Pate, Environmental and physiological controls over oxygen and carbon isotope composition of Tasmanian blue gum, *Eucalyptus globulus*. *Tree Physiol.* **25**, 129–146 (2005).
28. M. M. Barbour, G. D. Farquhar, Relative humidity- and ABA-induced variation in carbon and oxygen isotope ratios of cotton leaves. *Plant Cell Environ.* **23**, 473–485 (2000).
29. M. M. Barbour, J. S. Roden, G. D. Farquhar, J. R. Ehleringer, Expressing leaf water and cellulose oxygen isotope ratios as enrichment above source water reveals evidence of a Péclet effect. *Oecologia* **138**, 426–435 (2004).
30. G. D. Farquhar, L. A. Cernusak, B. Barnes, Heavy water fractionation during transpiration. *Plant Physiol.* **143**, 11–18 (2007).
31. R. F. Keeling, S. C. Piper, A. F. Bollenbacher, S. J. Walker, *Scripps CO₂ Program* (Scripps Institution of Oceanography, University of California, San Diego, La Jolla, CA, 2015).
32. M. A. Adams, T. N. Buckley, T. L. Turnbull, Diminishing CO₂-driven gains in water-use efficiency of global forests. *Nat. Clim. Chang.* **10**, 466–471 (2020).
33. M. Saurer *et al.*, Spatial variability and temporal trends in water-use efficiency of European forests. *Glob. Change Biol.* **20**, 3700–3712 (2014).
34. M. Wang, Y. Chen, X. Wu, Y. Bai, Forest-type-dependent water use efficiency trends across the Northern Hemisphere. *Geophys. Res. Lett.* **45**, 8283–8293 (2018).
35. A. Laverne *et al.*, Observed and modelled historical trends in water use efficiency of plants and ecosystems. *Glob. Chang. Biol.* **25**, 2242–2257 (2019).
36. B. E. Medlyn *et al.*, How do leaf and ecosystem measures of water-use efficiency compare? *New Phytol.* **216**, 758–770 (2017).
37. K. Yi *et al.*, Linking variation in intrinsic water-use efficiency to isohydricity: A comparison at multiple spatiotemporal scales. *New Phytol.* **221**, 195–208 (2018).
38. B. Choat *et al.*, Global convergence in the vulnerability of forests to drought. *Nature* **491**, 752–755 (2012).
39. J. S. Sperry, Evolution of water transport and xylem structure. *Int. J. Plant Sci.* **164**, S115–S127 (2003).
40. J. Carnicer, A. Barbato, D. Sperlich, M. Coll, J. Peñuelas, Contrasting trait syndromes in angiosperms and conifers are associated with different responses of tree growth to temperature on a large scale. *Front. Plant Sci.* **4**, 409 (2013).
41. W. K. Cornwell *et al.*, Climate and soils together regulate photosynthetic carbon isotope discrimination within C₃ plants worldwide. *Glob. Ecol. Biogeogr.* **27**, 1056–1067 (2018).
42. V. Haverd *et al.*, Higher than expected CO₂ fertilization inferred from leaf to global observations. *Glob. Chang. Biol.* **26**, 2390–2402 (2020).
43. K. A. Jennings, R. Guerrieri, M. A. Vadeboncoeur, H. Asbjørnsen, Response of *Quercus velutina* growth and water use efficiency to climate variability and nitrogen fertilization in a temperate deciduous forest in the northeastern USA. *Tree Physiol.* **36**, 428–443 (2016).
44. M. M. Savard, C. Bégin, M. Parent, A. Smirnov, J. Marion, Effects of smelter sulfur dioxide emissions: A spatiotemporal perspective using carbon isotopes in tree rings. *J. Environ. Qual.* **33**, 13–26 (2004).
45. S. A. M. McAdam, T. J. Brodribb, The evolution of mechanisms driving the stomatal response to vapor pressure deficit. *Plant Physiol.* **167**, 833–843 (2015).
46. C. Grossiord *et al.*, Plant responses to rising vapor pressure deficit. *New Phytol.* **226**, 1550–1566 (2020).
47. M. E. Duseney, A. G. Duarte, D. A. Way, Plant carbon metabolism and climate change: Elevated CO₂ and temperature impacts on photosynthesis, photorespiration and respiration. *New Phytol.* **221**, 32–49 (2019).
48. G. Battipaglia *et al.*, Elevated CO₂ increases tree-level intrinsic water use efficiency: Insights from carbon and oxygen isotope analyses in tree rings across three forest FACE sites. *New Phytol.* **197**, 544–554 (2013).
49. Q. Zhang *et al.*, Response of ecosystem intrinsic water use efficiency and gross primary productivity to rising vapor pressure deficit. *Environ. Res. Lett.* **14**, 074023 (2019).
50. T. J. Brodribb, S. A. M. McAdam, G. J. Jordan, S. C. V. Martins, Conifer species adapt to low-rainfall climates by following one of two divergent pathways. *Proc. Natl. Acad. Sci. U.S.A.* **111**, 14489–14493 (2014).
51. M. M. Barbour, Stable oxygen isotope composition of plant tissue: A review. *Funct. Plant Biol.* **34**, 83–94 (2007).
52. A. Kahmen *et al.*, Cellulose (δ)¹⁸O is an index of leaf-to-air vapor pressure difference (VPD) in tropical plants. *Proc. Natl. Acad. Sci. U.S.A.* **108**, 1981–1986 (2011).
53. L. Sternberg, P. F. V. Ellsworth, Divergent biochemical fractionation, not convergent temperature, explains cellulose oxygen isotope enrichment across latitudes. *PLoS One* **6**, e28040 (2011).
54. A. W. Cheesman, L. A. Cernusak, Infidelity in the feedback: Climate signal recorded in δ¹⁸O of leaf but not branch cellulose of eucalypts across an Australian aridity gradient. *Tree Physiol.* **37**, 554–564 (2017).
55. B. E. Medlyn *et al.*, Stomatal conductance of forest species after long-term exposure to elevated CO₂ concentration: A synthesis. *New Phytol.* **149**, 247–264 (2001).
56. H. Saxe, D. E. Ellsworth, J. Heath, Tree and forest functioning in an enriched CO₂ atmosphere. *New Phytol.* **139**, 395–436 (1998).
57. J. E. Campbell *et al.*, Large historical growth in global terrestrial gross primary production. *Nature* **544**, 84–87 (2017).
58. G. Forzieri, R. Alkama, D. G. Miralles, A. Cescatti, Response to Comment on "Satellites reveal contrasting responses of regional climate to the widespread greening of Earth." *Science* **360**, eaap9664 (2018).
59. H. D. Graven *et al.*, Enhanced seasonal exchange of CO₂ by Northern ecosystems since 1960. *Science* **341**, 1085–1089 (2013).
60. M. G. Ryan *et al.*, Transpiration and whole-tree conductance in ponderosa pine trees of different heights. *Oecologia* **124**, 553–560 (2000).
61. B. E. Ewers, S. T. Gower, B. Bond-Lamberty, C. K. Wang, Effects of stand age and tree species on canopy transpiration and average stomatal conductance of boreal forests. *Plant Cell Environ.* **28**, 660–678 (2005).
62. R. J. W. Brienen *et al.*, Tree height strongly affects estimates of water-use efficiency responses to climate and CO₂ using isotopes. *Nat. Commun.* **8**, 288 (2017).
63. C. D. Holmes, Air pollution and forest water use. *Nature* **507**, E1–E2 (2014).
64. P. Friedlingstein *et al.*, Global carbon budget 2019. *Earth Syst. Sci. Data* **11**, 1783–1838 (2019).
65. A. Rohatgi, WebPlotDigitizer: Web-based tool to extract data from plots, images, and maps, Version 4.2 (2019). <https://automeris.io/WebPlotDigitizer>. Accessed 15 July 2019.
66. C. Xu *et al.*, Increasing impacts of extreme droughts on vegetation productivity under climate change. *Nat. Clim. Chang.*, 10.1038/s41558-019-0630-6 (2019).
67. T. E. Huxman *et al.*, Convergence across biomes to a common rain-use efficiency. *Nature* **429**, 651–654 (2004).
68. C. MacFarling Meure *et al.*, Law Dome CO₂, CH₄ and N₂O ice core records extended to 2000 years BP. *Geophys. Res. Lett.* **33**, L14810 (2006).
69. I. C. Harris, P. D. Jones, CRU TS4.03: Climatic Research Unit (CRU) Time-Series (TS) Version 4.03 of High Resolution Gridded Data of Month-by-Month Variation in Climate (Jan. 1901–Dec. 2018) (Centre for Environmental Data Analysis, 2019).
70. G. Testa, F. Gresta, S. L. Cosentino, Dry matter and qualitative characteristics of alfalfa as affected by harvest times and soil water content. *Eur. J. Agron.* **34**, 144–152 (2011).
71. E. Dinerstein *et al.*, An ecoregion-based approach to protecting half the terrestrial realm. *Bioscience* **67**, 534–545 (2017).
72. F. Schweingruber, W. Landolt, The Xylem Database: A web product of the Swiss Federal Research Institute WSL (Swiss Federal Research Institute WSL, Birmensdorf, Switzerland, 2010). <https://www.wsl.ch/dendropro/xylemdb/>. Accessed 7 May 2019.
73. F.-W. Badeck, G. Tcherkez, S. Nogués, C. Piel, J. Ghashghaie, Post-photosynthetic fractionation of stable carbon isotopes between plant organs—a widespread phenomenon. *Rapid Commun. Mass Spectrom.* **19**, 1381–1391 (2005).
74. A. Gessler *et al.*, Stable isotopes in tree rings: Towards a mechanistic understanding of isotope fractionation and mixing processes from the leaves to the wood. *Tree Physiol.* **34**, 796–818 (2014).
75. N. Ubierna, G. D. Farquhar, Advances in measurements and models of photosynthetic carbon isotope discrimination in C₃ plants. *Plant Cell Environ.* **37**, 1494–1498 (2014).
76. A. Laverne *et al.*, Historical changes in the stomatal limitation of photosynthesis: Empirical support for an optimality principle. *New Phytol.* **225**, 2484–2497 (2019).
77. G. Farquhar, M. O'Leary, J. Berry, On the relationship between carbon isotope discrimination and the intercellular carbon dioxide concentration in leaves. *Aust. J. Plant Physiol.* **9**, 121–137 (1982).
78. D. McCarroll, N. J. Loader, Stable isotopes in tree rings. *Quat. Sci. Rev.* **23**, 771–801 (2004).
79. H. Craig, The geochemistry of the stable carbon isotopes. *Geochim. Cosmochim. Acta* **3**, 53–92 (1953).
80. G. D. Farquhar, J. R. Ehleringer, K. T. Hubick, Carbon isotope discrimination and photosynthesis. *Annu. Rev. Plant Physiol. Plant Mol. Biol.* **40**, 503–537 (1989).
81. C. J. Bernacchi, E. L. Singsaas, C. Pimentel, A. R. Portis, Jr, S. P. Long, Improved temperature response functions for models of Rubisco-limited photosynthesis. *Plant Cell Environ.* **24**, 253–259 (2001).
82. B. Stocker *et al.*, P-model v1.0: An optimality-based light use efficiency model for simulating ecosystem gross primary production. *Geosci. Model Dev. Discuss.* **37**, 1–59 (2019).
83. U. Seibt, A. Rajabi, H. Griffiths, J. A. Berry, Carbon isotopes and water use efficiency: Sense and sensitivity. *Oecologia* **155**, 441–454 (2008).
84. J. Flexas, M. Ribas-Carbo, A. Diaz-Espejo, J. Galmés, H. Medrano, Mesophyll conductance to CO₂: Current knowledge and future prospects. *Plant Cell Environ.* **31**, 602–621 (2008).
85. M. M. Barbour, T. J. Andrews, G. D. Farquhar, Correlations between oxygen isotope ratios of wood constituents of *Quercus* and *Pinus* samples from around the world. *Aust. J. Plant Physiol.* **28**, 335–348 (2001).
86. G. J. Bowen, J. B. West, C. C. Miller, L. Zhao, T. Zhang, IsoMAP: Isoscapes modeling, analysis and prediction, Version 1.0. The IsoMAP Project (2020). <https://isomap.org>. Accessed 18 September 2020.
87. Lda. S. Sternberg, M. J. Deniro, R. A. Savidge, Oxygen isotope exchange between metabolites and water during biochemical reactions leading to cellulose synthesis. *Plant Physiol.* **82**, 423–427 (1986).
88. S. Belmecheri, W. E. Wright, P. Szejner, K. A. Morino, R. K. Monson, Carbon and oxygen isotope fractionations in tree rings reveal interactions between cambial phenology and seasonal climate. *Plant Cell Environ.* **41**, 2758–2772 (2018).
89. K. Treydte *et al.*, Seasonal transfer of oxygen isotopes from precipitation and soil to the tree ring: Source water versus needle water enrichment. *New Phytol.* **202**, 772–783 (2014).
90. J. Pinheiro, D. Bates, S. DebRoy, D. Sarkar, R Core Team, nlme: Linear and nonlinear mixed effects models. R package, Version 3.1-131.1 (2018). <https://CRAN.R-project.org/package=nlme>. Accessed 15 July 2019.
91. V. M. R. Mugge, segmented: An R package to fit regression models with broken-line relationships. *R News* **8/1**, 20–25 (2008).
92. K. Bartoň, MuMIn: Multi-model inference. R package, Version 1.40.0. (2017). <https://cran.r-project.org/web/packages/MuMIn/index.html>. Accessed 15 July 2019.
93. H. Schielzeth, Simple means to improve the interpretability of regression coefficients. *Methods Ecol. Evol.* **1**, 103–113 (2010).
94. P. Breheny, W. Burchett, Package "visreg": Visualization of regression models. *R J.* **9**, 56–71 (2017).
95. R. Mac Nally, C. J. Walsh, Hierarchical partitioning public-domain software. *Biodivers. Conserv.* **13**, 659–660 (2004).
96. K. Murray, M. M. Conner, Methods to quantify variable importance: Implications for the analysis of noisy ecological data. *Ecology* **90**, 348–355 (2009).
97. R. Lenth, emmeans: Estimated marginal means, aka least-squares means. R package, Version 1.4.3.01 (2019). <https://cran.r-project.org/web/packages/emmeans/index.html>. Accessed 15 July 2019.
98. T. Hothorn, F. Bretz, P. Westfall, Simultaneous inference in general parametric models. *Biom. J.* **50**, 346–363 (2008).